

HIGH-RATE GNSS TECHNIQUES FOR THE DETECTION OF LARGE SEISMIC DISPLACEMENTS

T. Ning, J.M. Johansson, H.-G. Scherneck

Chalmers University of Technology
Department of Radio and Space Science
Onsala Space Observatory
SE-439 92 Onsala, Sweden

P.O.J. Jarlemark, R. Emaradson

SP Technical Research Institute of Sweden
Box 857
SE-501 15 Borås, Sweden

ABSTRACT

Measurement of co-seismic strong-motion displacements at sub-second temporal resolution is of great importance for earthquake studies. We have investigated the usage of high-rate sampled Global Navigation Satellite System (GNSS) data to measure seismic motion by implementing an industrial robot simulating the displacements close to an earthquake epicenter. The robot arm is tracked by GNSS signals. Two baselines—400 m and 60 km—from the robot to reference stations are used to process the observed GPS data. Both methods give similar (within 0.5 mm) Root Mean Square (RMS) differences between the estimated and the commanded coordinates. The RMS differences are 3.5 mm in the east component, 5.6 mm in the north component, and 8.1 mm in the vertical component.

Index Terms— Seismic strong motion, GNSS, GPS

1. INTRODUCTION

Seismic strong motion is the surface displacements that occurs in the vicinity of earthquake epicenters. The detection of the near-field deformation is important for determining parameters of the seismic source and for providing engineers with information in order to improve earthquake resistance for buildings and other structures. Usually strong-motion observations in seismology are based on accelerometers, and displacements can be derived from double time-integrated accelerograms [1]. Glitches in the sensor (mostly due to the rotation of the instrument out of the set orientation, leading to cross-talk between the channels), however may occur during the most intense period of the shaking. As the result, the derived displacements deviate from the truth. Due to the fact that the antenna position would be much less susceptible to rotation components in the shaking (except for rotations around a horizontal axis if the antenna is on a tower), and displacements are dominated by low-frequency signals, they can be observed at a few Hz by GNSS observations. If the installation of the GNSS antenna is sufficiently stable,

displacements of earthquakes can be recorded and estimated with rather small uncertainty and without losing time resolution. The use of 1-Hz GPS data to estimate the seismic displacement has been successfully demonstrated in several studies [2], [3]. They found that the vertical component was too noisy for a significant reduction of variance when synthetic waveforms were fitted to and subtracted from the signal. Therefore, it is interesting to investigate the usage of high-rate sampled GNSS data.

In this study, a GNSS receiver with a high-rate sampling of 20 Hz was used with an industrial robot which was installed to simulate displacements of an earthquake (see Figure 1). The recording from the Michoacan, earthquake in Mexico, was chosen as the reference data. The earthquake happened at 13:18 UTC, September 19th, 1985, N17.910 W101.909. The accelerometer data in 3-components (east, north, and vertical) at 200 smp/s was provided by the COSMOS Virtual Data Centre [4] Caleta de Campos, Mexico, N18.073, W102.55 at 15 km distance from the epicenter. The Moment Magnitude (M_w) was 8.0 (USGS National Earthquake Information Center [5]). We describe the GPS data acquisition and analysis in Sections 2 and 3, respectively. In Section 4, we present the results followed by the conclusions in Section 5.

2. GPS DATA ACQUISITION

Currently there are more than 30 GPS satellites orbiting the earth at an altitude close to 20,200 km. All GPS satellites are distributed evenly into 6 nearly circular orbital planes with an inclination angle of 55° and with a 12 h orbital period. GPS signals are transmitted at two frequencies, L1 at 1575.42 MHz and L2 at 1227.60 MHz. The timing of radio signals propagating between the satellites and the ground-based GPS receivers is the fundamental observable. With carrier phase observations, high-accuracy positioning can be obtained [6]. The antenna in this study has the capability to receive both the GPS carrier frequencies (L1 and L2), and the frequencies from the GLObalnaja NAVigatsionnaja Sputnikovaja Sistema (GLONASS). A choke ring assembly was equipped to



Fig. 1. The installation of a GPS antenna mounted on an industrial robot simulating the displacement of the earthquake.

the antenna to reduce multipath effects [7]. The robot was programmed to move along a trajectory specified by 254 positions. To be easier to design the movement of the robot, we have subtracted out a ramp. In reality there is a large offset between the beginning and the end of the series where the quiet end is parallel to the time axis. The movement was divided into 0.2 s long intervals, of which the robot moved to the next position during 0.1 s and rested for the remaining 0.1 s. After completing the whole trajectory (51 s), the robot was static for 309 s before performing a new 6 minute cycle, resulting in 10 cycles per hour. To be able to acquire sufficient number of data points, to track the movement of the robot, the sampling rate of the GPS receiver was set to 20 Hz. Data with the same sampling rate from two other sites in the International GNSS Service (IGS) network [8] were used as reference. One is the ONSA station which is approximately at a 400 m distance from the robot antenna. The other station, SPT0 is about 60 km away. Thus a short baseline (robot-ONSA) and a long baseline (robot-SPT0) are available for signal processing. In total, 30 cycles (3 h of observations starting at 12:00 local time, March 11th, 2009) were carried out.

3. GPS DATA ANALYSIS

The acquired data were processed using an in-house Matlab-based GNSS software package to estimate the state variables, namely the east, north, and vertical displacements of the antenna. The main approach is parameter elimination where "single differences" of the carrier phase measurements are used as observables, and modeled as:

$$\phi = R - I + Z + \lambda N + c\tau_s - c\tau_r + \epsilon \quad (1)$$

where R is the true range between a receiver and a satellite, I is the ionospheric delay, Z is the delay from the neutral atmosphere, N is the ambiguity that is an unknown number of complete cycles between the satellite and the receiver, τ_s and τ_r are the satellite and the receiver clock term respectively, and ϵ is the observation noise. A single difference of the carrier phase measurement between two receivers observing the same satellite can be formed as

$$\Delta\phi = \Delta R - \Delta I + \Delta Z + \lambda\Delta N + c\Delta\tau_r + \Delta\epsilon \quad (2)$$

We note that the single difference is free from the satellite clock error (τ_s). In addition, the single difference of the carrier phase measurements (L1 or L2) has lower noise than the corresponding combined observations (L3), but with ionospheric irregularity residing in the phase difference. In this work, we mainly chose L1 observations as the fundamental measurements due to relatively great influence on L2 from reflections of the mechanical structure.

3.1. Short baseline

Because of the short baseline (400 m), the ionospheric influence on the signal from a satellite is nearly identical, and can be effectively eliminated by the single difference technique. The differential neutral atmospheric delay can also be ignored for the horizontal part. However, a compensation for the vertical part has to be made due to the altitude difference between the antennas. Using satellite data from broadcast ephemerides the doppler shift can be calculated. In addition, a correction was made for the two receiver antennas differences in phase pattern using the IGS models [9]. A reliable ambiguity fixing can be made after elimination of the main systematic effects, i.e. the atmosphere and the satellite orbit errors. Finally, the ambiguity fixed data were put into a discrete Kalman filtering algorithm for the estimation of the coordinates. The estimates were smoothed backwards in time using the Rauch-Tung-Striebel algorithm [10].

3.2. Long baseline

Unlike the short baseline, the atmospheric delays will be significantly different between two stations separated by 60 km. Instead of eliminating those delays, we can actually estimate the linear trend of the combination of all uncertainties for each satellite, i.e. ionosphere, neutral atmosphere, tide effects and ambiguity. For each epoch (0.05 s) we processed the GPS data with two additional parameters (the linear trend and the variance of the trend) of the combined uncertainties for each satellite. We run a solution forward in time, and one solution backwards in time, independent of each other, and then combine the results [11].

The elevation-dependent unmodelled error, i.e. multipath reflection [12], due to the surrounding environment of the

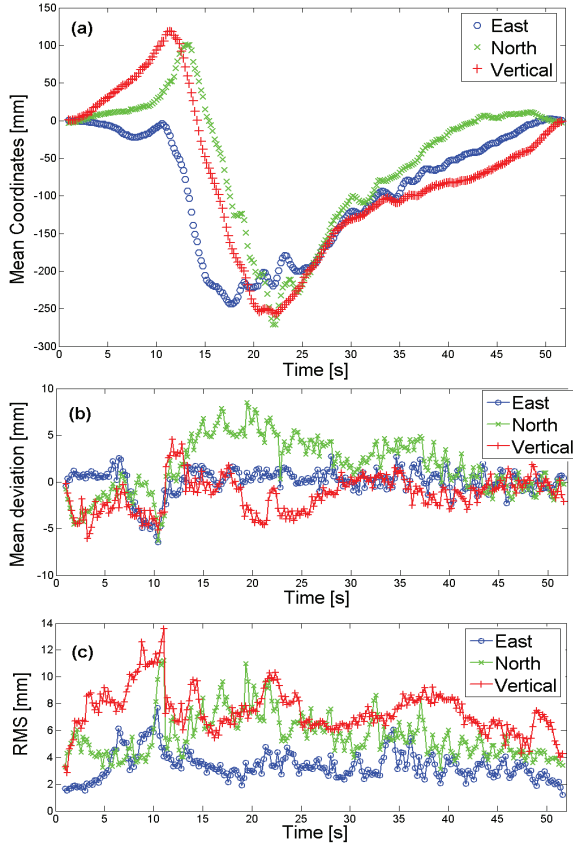


Fig. 2. Results derived from the long baseline processing. (a) The commanded robot coordinates, (b) the mean deviations, and (c) the mean RMS differences between the estimated and the commanded coordinates based on 30 cycles.

GPS antennas is one significant error source. It can be mitigated by attaching anti-reflection material to the GPS antenna [13] or by setting a higher elevation cutoff angle for the data analysis. In this work, data below 15° were eliminated. For higher elevation cutoff angles it might be good to include more measurements in the data analysis. To investigate the influence of the number of measurements on the results, in addition to using only L1 measurements in the data analysis we also use both L1 and L2 measurements as independent measurements (but give the L2 measurements slightly smaller weights because of their higher noise). We also use both GPS and GLONASS data.

4. RESULTS AND DISCUSSION

Figure 2 shows the results in the estimated coordinates obtained from the GPS data derived from the long baseline processing (the short baseline processing gives almost identical patterns and results). As shown in Figure 2, the estimated values from the GPS data are highly correlated to the com-

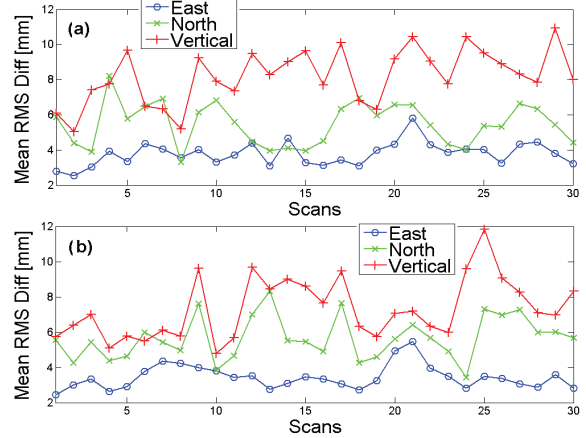


Fig. 3. Mean RMS differences in estimated coordinates and commanded robot positions for each scan. The results are derived from (a) the short baseline processing and (b) the long baseline processing.

manded robot positions for all three components (east, north, and vertical). In Figure 2b, we note that the estimated horizontal components have smaller deviations than the vertical part. The Root Mean Square (RMS) differences between the estimated and the commanded coordinates are shown in Figure 2c. The short baseline processing gives similar (RMS differences within 0.5 mm) results. The RMS differences are 3.5 mm in the east component, 5.6 mm in the north component, and 8.1 mm in the vertical component. We also investigated the stability of the data processing by studying the RMS differences for each scan between the estimated and the commanded coordinates (see Figure 3). As shown in Figure 3, RMS differences in the east component (for both baselines) behave more stable than the other two components where the vertical part has the highest variability.

In Figure 4, mean RMS differences and variabilities for the RMS values caused by different inputs to the data analysis are illustrated. Using both GPS L1 and L2 reduced the RMS differences by approximately 4% for the horizontal components, and 2% for the vertical components. These percentages of improvement became 8% and 4% when including the GLONASS L1 data in the analysis. The use of the GLONASS L2 data did not have any influence. However, these results are based on the fact that a significant part of the GPS L2 and GLONASS observations were missing due to receiver problems. When sampling with 20 Hz, the receiver was too busy to write all data in its internal memory, and stream data to a PC at the same time. Hence, further studies using more observations are recommended.

It should be mentioned here that due to the mechanical instability in the mount of the robot, the movement of the robot probably would not follow the commanded positions exactly. Then the current RMS differences might not reflect the true

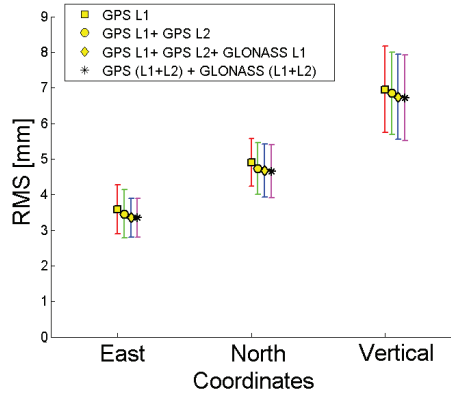


Fig. 4. The mean RMS differences obtained by only using GPS L1 measurements (squares), GPS L1 and L2 measurements (circles), GPS L1 and L2 plus GLONASS L1 measurements (diamonds), and GPS L1, L2 plus GLONASS L1, L2 measurements (stars). The results are derived from the long baseline processing and 30 cycles. Errorbars denote the standard deviation around the average.

deviations of GNSS estimates, and some contribution is expected from the robot positions. Independent data from additional position sensors and motion detectors such as a laser tracker or an Inertial Measurement Unit (IMU) can be used to track the 3D coordinates of the robot movement with high accuracy (less than tenths of a millimeter). We have included the IMU in our newest measurement, and the data processing is ongoing. Eventually, by implementing the calibrated robot positions from the sensor measurement, the errors in the GNSS estimates can be correctly identified.

5. CONCLUSIONS

We have shown that GNSS data can monitor rapid motion over time scales of seconds with a repeatability at the millimeter level. We also have shown that atmospheric delays affecting the GPS data can be absorbed either by the single difference technique (short baseline processing), or were estimated with other irregularities, i.e. ambiguities and tide effects together (long baseline processing). Therefore, accurate modeling of individual errors in the GPS observations is not necessary. Both baselines give smaller RMS differences from the commanded robot positions for the estimated horizontal components. The larger differences obtained in the vertical component are due to the geometry. Using more measurements (GPS L1, L2, and GLONASS L1) may improve the results slightly. However, the current results need to be further investigated by implementing extra sensors to monitor the movement of the robot, in order to determine its contribution to the observed deviations.

6. REFERENCES

- [1] J.G. Anderson, Lee. W.H.K., H. Kanamori, P.C. Jennings, and Kisslinger, "International handbook of earthquake and engineering seismology," *Academic Press*, pp. 937–966, 2003.
- [2] G.L. Emore, J.S. Haase, K. Choi, K.M. Larson, and A. Yamagiwa, "Recovering seismic displacements through combined use of 1-Hz GPS and strong-motion accelerometers," *BSSA*, vol. 97, no. 2, pp. 357–378, 2007.
- [3] R. Kobayashi, S. Miyazaki, and K. Koketsu, "Source processes of the 2005 West Off Fukuoka Prefecture earthquake and its largest aftershock inferred from strong motion and 1-Hz GPS data," *Earth Planets Space*, vol. 58, pp. 57–62, 2006.
- [4] "<http://www.cosmos-eq.org/>," .
- [5] "<http://neic.usgs.gov/>," .
- [6] B.W. Remondi, "Global positioning system carrier phase: description and use," *Bull. Geod.*, vol. 59, no. 4, pp. 361–377, 1985.
- [7] J.M. Tranquilla, J.P. Carr, and H.M. Al-Rizzo, "Analysis of a choke ring groundplane for multipath control in Global Positioning System (GPS) applications," *IEEE Trans. Ant and Propag.*, vol. 42, no. 7, pp. 905–911, 1994.
- [8] "<http://igsceb.jpl.nasa.gov/network/list.html>," .
- [9] "<http://igsceb.jpl.nasa.gov/igsceb/station/general/igs05.atx>," .
- [10] H.E. Rauch, F. Tung, and C.T. Striebel, "Maximum likelihood estimates of linear dynamic systems," *AIAA*, vol. 3, no. 8, pp. 1445–1450, 1965.
- [11] D.C. Fraser and J.E. Potter, "The optimum linear smoother as a combination of two optimum linear filters," *IEEE Trans. Automat Contr.*, vol. 14, no. 4, pp. 387–390, 1969.
- [12] P. Elosegui, J.L. Davis, R.T.K. Jaldehag, J.M. Johansson, A.E. Niell, and I.I. Shapiro, "Geodesy using the global positioning system: the effects of signal scattering on estimates of site position," *J. Geophys. Res.*, vol. 100, no. 6, pp. 921–934, 1995.
- [13] C. Granström, "Site-dependent effects in high-accuracy applications of GNSS," *Ph.D. thesis, Chalmers University of Technology, Göteborg*, 2006.